London Road, Bracknell
Berkshire RG12 2SZ

LONDON, METEOROLOGICAL OFFICE.
Met.O.11 Technical Note No.256

Experiments with divergence damping and reduced diffusion in the mesoscale model.

MET O 11 TECHNICAL NOTE NO 256

EXPERIMENTS WITH DIVERGENCE DAMPING AND REDUCED DIFFUSION IN THE MESOSCALE MODEL

S.P. BALLARD

Meteorological Office, Bracknell, UK

Met O 11 (Forecasting Research)
Meteorological Office
London Road
Bracknell
Berkshire
England

May 1987

EXPERIMENTS WITH DIVERGENCE DAMPING AND REDUCED DIFFUSION IN THE MESOSCALE MODEL

1. Introduction

Operationally the mesoscale model is run with various forms of smoothing and diffusion included. In order to stabilize the leap-frog time scheme and sound waves in the model , time-smoothing is used and , in order to cope with the nonlinear instability and perhaps other effects, horizontal diffusion is applied. The values of these diffusion coefficients appear to be extremely high. In particular the horizontal diffusion of momentum will smooth two grid length waves on a time scale of 500secs (approximately 10 timesteps) and 10 gridlength waves (150km) in 4 hours. In order to obtain tighter gradients or smaller scale details in the model , experimental forecasts have been run with lower diffusion coefficients. Also it has been found that it is possible to run the operational fine-mesh model with reduced horizontal diffusion by including divergence damping (Dumelow 1983 , Dickinson and Gange 1985) thus producing smoother vertical velocity fields and suppressing noise in the precipitation fields and surface pressure tendency. Thus we have studied the effects of divergence damping and reduced horizontal diffusion in the mesoscale model. In section 2 the forms of explicit diffusion and smoothing implemented in the formulation of the mesoscale model are described. Then in section 3 divergence damping and its form of implementation in the mesoscale model is described. In sections 4 and 5 the results of two case studies with varying levels of diffusion are described and the conclusions are discussed in section 6.

2. Forms of Diffusion and Smoothing in the Mesoscale Model

There are three basic forms of diffusion or smoothing employed in the mesoscale model. These are time smoothing , linear horizontal diffusion and the use of a turbulence scheme for the vertical fluxes or vertical diffusion to define the degree of turbulent mixing.

2.1 Time smoothing

In order to dampen the splitting of computational and physical mode solutions obtained using a leap-frog (centred time, centred space) finite difference scheme, time smoothing is applied to the fields of forecast variables.
An Asselin time filter is applied to the fields so that for field A

$$A^{*t} = A^{t} + \epsilon \left(A^{*t-\Delta t} - 2A^{t} + A^{t+\Delta t} \right)$$

where A can be u, v, etadot, P, θ, TKE, q, m, T_s and T_g (see Appendix A) and an asterix implies that the field has been time smoothed.

A value of $\epsilon = 0.2$ is used.

Until recently m was not time smoothed but it was found that roughnesses in the precipitation field, produced when the level of horizontal diffusion was decreased, were greatly reduced once the cloud water field was time smoothed. Possibly it would be more correct to time smooth the total water variable, which is the advected variable , rather than the cloud water and water vapour separately.

Time smoothing also helps (Carpenter 1979) to dampen the 4-timestep unstable sound waves produced as a result of violating the stability criterion for sound waves (Tapp and White 1976).

$$N^2 \times \Delta t^2 < 1$$

The operational value of the timestep (60secs) has been chosen to cope with the normal values of N^2.The value of ϵ was increased in December 1985 from 0.1 in order to obtain successful forecasts when high values of N^2 (such as those resulting from low tropopause heights on 11/4/85) are found in the model domain (top at 12km). This has not provided stability in all cases , such as the week-end of 23/3/86 . Stability can be maintained in that case by reducing the time-step or using a forward (rather than centred) weighting in the implicit scheme for the sound waves. The latter was implemented in the mesoscale model from December 1986.
Carpenter (1979) used a value of ϵ=0.02 but his upper boundary was at 4km so that the maximum value of N^2 was likely to have been smaller. We also note that Tripoli and Cotton (1982), who use a split method using shorter timesteps for the acoustic terms but a leap-frog scheme for the remaining terms , use a value of ϵ=0.1.

All forecasts described in this paper use ϵ=0.2 and the centred implicit scheme and include time smoothing of the cloud water field.

2.2 Linear Horizontal Diffusion

It has been found to be essential to include some form of horizontal diffusion of the u,v,θ_L and q_t fields in order to obtain successful integrations of the model.
Originally nonlinear diffusion was used in the mesoscale model but following the work of Parrett and Cullen 1984 the formulation was changed to linear thus providing a saving in cpu time (Machin 1983).
At present this is of the form

$$dA/dt = K_{hor} DEL^2_H A$$

where $DEL^2_H = d^2/dx^2 + d^2/dy^2$

and $K_{hor} = K_M = 4.5 \times 10^4$ m^2 s^{-1} for u and v

and $K_{hor} = K_H = 2.25 \times 10^4$ m^2 s^{-1} for θ_L and q_t

Until recently $K_M = K_H = 4.5 \times 10^4$ m^2 s^{-1} but the value of KH was reduced as a result of the experiments described in sections 4 and 5.

Using the forward time (over $2\Delta t$) , centred space formulation for the diffusion equation in two dimensions , as in the mesoscale model, gives the stability criterion

$$K_{hor} \times (2\Delta t/\Delta x^2) \leq 1/4$$

That is a maximum allowed value of $K_{hor} = 4.7 \times 10^5$ m^2 s^{-1} when Δt = 60 sec and Δx = 15km.
Values of the model variables are given on eta surfaces , that is height above model orography. Diffusion of u and v is applied along eta surfaces so that the finite difference approximation is

using notation

$$A_x = (A(x+\Delta x/2) - A(x-\Delta x/2))/\Delta x$$

$DEL^2_H A = A_{xx} + A_{yy}$, where A = u or v

For the θ_L field it has been found to be essential to apply the diffusion along approximately horizontal surfaces (Bailey 1982). Otherwise the vertical stratification of potential temperature will contribute to the diffusion in the vicinity of hills. The diffusion of q_t is also performed along approximately horizontal surfaces. This is achieved by correcting adjacent values to the same height above mean sea level before calculating the derivatives.

Consider diffusion at grid point i in the x direction over three successive grid points of heights E(i-1), E(i) , E(i+1).
At a given eta level k the field A has values A(i-1,k), A(i,k) and A(i+1,k). The values of A(i-1,k) and A(i+1,k) are corrected to height eta(k) + E(i) so that

$$A'(i-1,k) = A(i-1,k) - \frac{(E(i-1)-E(i))(A(i-1,k+1)-A(i-1,k-1))}{eta(k+1)-eta(k-1)}$$

$$A'(i+1,k) = A(i+1,k) - \frac{(E(i)-E(i+1))(A(i+1,k+1)-A(i+1,k-1))}{eta(k+1)-eta(k-1)}$$

When k=1 the vertical interpolation is calculated over levels k+1 and k rather than k+1 and k-1. This formulation may still cause problems when the difference in orographic heights at successive grid points is greater than the difference in heights of the eta levels used in the vertical gradient calculation. It then becomes an extrapolation rather than an interpolation formula. Thus it may be better to diffuse along eta surfaces in the boundary layer, where the model level spacing is small and only along approximately horizontal surfaces in the free atmosphere. Alternatively it may be possible to remove the lateral diffusion altogether in the boundary layer. The latter option is tried in section 5.

2.3 Turbulence Scheme and Vertical Diffusion

The turbulence scheme is described in Smith (1984 a and b).

Basically an implicit scheme is used to solve the equation

$$dA/dt = d\,(\,K\,dA/deta\,)/\,deta$$

where A is u, v, θ_L, q_t or TKE

and K = K_m , K_h or K_e = f(TKE , N^2 , S^2 , l)

where l is a length scale defined by

$$1/l = 1/(kz) + 1/\lambda$$

with k=0.4 = Von Karman's constant

and $\lambda = \alpha\, h$ with $\alpha = 1/6$

h is the depth of the layer with significant TKE (ie TKE $> 10^{-3}$) containing the level at which K is required . So at upper levels h is at least the depth of one layer and in the boundary layer h will be of the order of the boundary layer depth.

Vertical diffusion of the vertical velocity etadot is also performed using an equation of the form

$$d(etadot)/dt = |\,d(etadot)/deta\,|\,d^2(etadot)/deta^2$$

3. Divergence Diffusion

Divergence diffusion or, as it is alternatively known, divergence damping is used in the operational assimilation and fine-mesh models to reduce noise and roughnesses (Dumelow 1983 , Dickinson and Gange 1985). Experimental forecasts with a 37km version of the fine-mesh model required divergence damping in order that roughnesses in the vertical velocity field could be removed so that cross frontal circulations could be studied.
The form of diffusion is such that equations of the form

$$du/dt = K_D\, dD/dx \;,\; dv/dt = K_D\, dD/dy$$

where $D = du/dx + dv/dy$

are solved giving

$$dD/dt = K_D\, DEL^2 D$$

ie divergence diffusion.

In the operational fine-mesh and assimilation models and also the hemispheric coarse-mesh models used in the fine-mesh forecasting suite the divergence damping is applied at each of the adjustment steps of the integration, there being three adjustment steps to each advection step. The value of K_D varies so that

$K_D = 5 \times 10^6\ m^2\ s^{-1}$ for the hemispheric forecast

$= 2.5 \times 10^6\ m^2\ s^{-1}$ for the assimilation cycle

$= 2.5 \times 10^6\ m^2\ s^{-1}$ reducing to

$1.0 \times 10^6\ m^2\ s^{-1}$ over the first six hours of the fine-mesh forecast

The operational models also use nonlinear horizontal diffusion of the form

$$dA/dt = K\,|\,DEL^2\,A\,|\,DEL^2\,A$$

where $K = 2.5 \times 10^{13}\ m^4\ s^{-1}$ for θ, u and v in the fine-mesh model

and $K = 2.5 \times 10^{16}\ m^4\ s^{-1}$ for q in the fine-mesh model

Recently (Bell and Downton 1986) trial coarse-mesh forecasts with reduced nonlinear diffusion and including divergence damping have been run. The aim was to try to increase the forecast jet speeds. Sensitivity tests suggested suitable values of K and K_D as $4 \times 10^{13}\ m^4\ s^{-1}$ and $1 \times 10^6\ m^2\ s^{-1}$ respectively. With these coefficients a modest increase in forecast jet speed was obtained but verification of forecasts for greater than 48 hours ahead verified worse than the operational model.

Following the experiences with the operational forecast model it was decided to study the impact of divergence damping on the mesoscale model.

3.1 Implementation of Divergence Damping in the Mesoscale Model

We need to add terms of the form

$$K_D\, dD/dx \text{ and } K_D\, dD/dy$$

to the tendencies for the u and v components of velocity respectively.

On an Arakawa C grid the divergence D is best described at pressure points and the gradients of divergence at the corresponding velocity points (see figure 1).

So that for $D = du/dx + dv/dy$

using notation $A_x = (A(x+\Delta x/2) - A(x-\Delta x/2))/\Delta x$

$$D = u_x + v_y$$

and $K_D\ dD/dx = K_D\ D_x = K_D\ (u_{xx} + v_{yx})$

and $K_D\ dD/dy = K_D\ D_y = K_D\ (u_{xy} + v_{yy})$

This form of diffusion is applied along eta levels as is done in the normal diffusion of u and v.

4. 06z 11/4/85 Case Study

Various runs of the mesoscale model were made with 06z surface observations analysed and merged into a T+6 interpolated fine-mesh forecast for 06z 11/4/85. This forecast sucessfully completed 12 hours using the original operational values of $K_M = K_H = 4.5 \times 10^4\ m^2\ s^{-1}$ and no divergence damping.
However a test integration with $K_M = K_H = 4.5 \times 10^3\ m^2\ s^{-1}$ and no divergence damping failed after 5 hours. Thus various runs were made including divergence damping using different values of the divergence damping coefficient K_D to see if its inclusion would produce a successful forecast.
Three values were used $K_D = 1 \times 10^4$, 1×10^5 and 1×10^6 respectively with $K_H = K_M = 4.5 \times 10^3$. A successful 12 hour run was obtained using $K_D = 1 \times 10^5$ but the runs with $K_D = 1 \times 10^4$ and $K_D = 1 \times 10^6$ failed after nearly 6 hours and 26 steps respectively. Thus it seems that we need a value of K_D greater than 1×10^4 but less than 1×10^6, the latter value probably violates the stability criterion as it will be similar to that for the diffusion equation given in section 2.2.

4.1 Synoptic Situation

At 06z on 11/4/85 a low of analysed centre 990mb was positioned over the Irish Sea with an associated occlusion through south east Scotland , a warm front into the south west of England and a cold front just off the South West Penninsula. The low deepened to 982 mb and moved to a centre just north of East Anglia by midday with its associated occluded fronts having a north-south orientation. There was persistent and at times heavy rain associated with the fronts and behind the fronts there were many heavy showers with some hail.
Unfortunately the 00z 11/4/85 fine-mesh forecast used as the background for the initial and boundary conditions produced an erroneous evolution as it did not produce the low centre in the Irish Sea at 06z. This had an adverse effect on the accuracy of the mesoscale forecast so we will not compare the forecasts with observations.

4.2 Comparison of 09z (T+3) forecasts

Table 1 shows the combination of values of the coefficients K_M, K_H and K_D tried in a series of experimental 3 hour forecasts and they will be referred to by their index letters A1 to E1 in the following text.

Table 1. Experimental T+3 forecasts for 09z 11/4/85

INDEX	K_H	K_M	K_D
A1	4.5×10^4	4.5×10^4	0
B1	2.25×10^4	4.5×10^4	0
C1	4.5×10^3	4.5×10^3	0
D1	4.5×10^3	4.5×10^3	10^4
E1	4.5×10^3	4.5×10^3	10^5

Figures 2 and 3 show the comparison of the forecasts of mean sea level pressure, 10m wind, dynamic and convective precipitation and visibility for experiments A1 to E1. It can be seen from figure 2 that as K_H and K_M are reduced the fields become rougher, particularly the distribution of convection and the mean sea level pressure in the region of the convection. The convection is generally less organised with lower diffusion. Also as expected the stratiform rain field is less smooth with lower diffusion but features such as the clearance between the frontal band and the area of convection and stratiform precipitation in the trough may be adding detail to the forecast. There is no evidence of sharpening of the trough in the wind or pressure fields as the level of diffusion is reduced. This is probably due to the dominant influence of the moist processes in the model.
The impact of various levels of divergence damping on the forecast is shown in figure 3. It can be clearly seen that as the value of K_D is increased the fields become smoother. In fact the forecast with $K_D = 10^5$, expt. E1 ,is almost as smooth as that from the operational run A1. The only significant difference is the greater area of clearance of stratiform precipitation in expt. E1.

Cross-sections of vertical velocity, potential temperature and convecting levels and grid points are shown in figure 5 for experiments A1,C1,D1 and E1. The line of cross-section is shown in figure 4. It is again evident that the fields are rougher, with shorter wavelength features, and the vertical velocities more intense at lower levels of diffusion. It is noticeable that the roughness is far worse in the regions of convection in the west of the cross-section. The frontal region in the east has similar scale in all experiments , the only main

differences being the increase in magnitude of the vertical velocity at lower levels of diffusion. The comparison of figure 5 a),b) and c) shows that as the level of divergence damping is increased the vertical velocity field becomes smoother. Again, as with the surface charts, there is very little difference between expt E1 and A1.Reducing the level of horizontal diffusion has very little impact on the potential temperature field , apart from changes resulting from rougher vertical velocity fields. This may be a result of limitations on gradients imposed by the vertical resolution of the model.

5. 06z 17/6/86 Case Study

The second case studied in these diffusion experiments is a three hour forecast from 06z on 17/6/86. This case was studied because in the operational trial the mesoscale model had produced a good temperature forecast, correctly producing a contrast between high temperatures of 25 deg C in East Anglia and low temperatures of about 11 deg C on the west coast of Wales. This meant that the impact of reducing levels of diffusion on the screen level temperature and cloud could be studied, especially in mountainous regions.

As with the 11/4/85 case various runs of the mesoscale model were made with various values of K_M,K_H and K_D. The initial conditions were those produced operationally consisting of 06z observations analysed and merged into a hybrid dataset combined from a T+6 interpolated fine-mesh forecast and a T+3 mesoscale forecast, see figure 6. The operational run successfully completed 12 hours with $K_M = K_H = 4.5 \times 10^4$ and $K_D = 0$.

Table 2 shows the combination of values of the coefficients K_M, K_H and K_D tried in a series of experimental 3 hour forecasts and they will be referred to by their index letters A2 to I2 in the following text.

Table 2. Experimental T+3 forecasts for 09z 17/6/86

Index	K_H levels 1-3	K_H levels 4-16	K_M	K_D	length of successful forecast (1min steps)
A2	4.5×10^4	4.5×10^4	4.5×10^4	0	> 180
B2	0	4.5×10^4	4.5×10^4	0	> 180
C2	2.25×10^4	2.25×10^4	4.5×10^4	0	> 180
D2	0	0	4.5×10^4	0	> 180
E2	4.5×10^3	4.5×10^3	4.5×10^3	0	98
F2	4.5×10^3	4.5×10^3	4.5×10^3	10^5	> 180
G2	0	4.5×10^3	4.5×10^3	10^5	> 180
H2	0	0	0	10^5	> 180
I2	0	0	1×10^4	10^4	121

From studying table 2 it appears that in order to obtain a successful forecast (in this case a successful forecast is one that reaches 180 steps ie 3 hours) a minimum level of horizontal diffusion of momentum is required. This can either be in the form of linear diffusion or divergence damping but a coefficient of greater than about 4.5×10^4 is required. Model failures, when they occurred were in the form of grid point instability in the region of convection and precipitation off the south east coast of Scotland. It is also clear from table 2 that forecasts can be successfully run with no diffusion of the thermodynamic variables θ_L and q_t.

Comparison forecasts with the horizontal diffusion of θ_L and q_t removed in the bottom three levels were also run in order to study the effects of the problem of trying to calculate the diffusion along approximately horizontal surfaces near steep orographic gradients.

5.2 Synoptic Situation

A weak cold front lying north east to south west moved eastwards over the UK during the day. The analysed position at 09z is shown on the British Isles chart in figure 7. when there was a low of 1008mb central pressure over the Pennines. Most of England had a good deal of sunshine after the clearance of early morning mist. In southern and eastern Scotland it was cloudy with outbreaks of rain which were heavy at times and there were several thunderstorms. From figure 7 we can see that at 09z there were reports of light rain and drizzle from central Scotland, Northern Ireland, the Isle of Man and west Wales. Showers were reported in the Republic of Ireland and thunderstorms had been reported in the past hour in south east Scotland. Fog was reported on the Channel coasts and the east coast of Scotland. There were clear skies in eastern England with temperatures reaching 25 deg C in parts of East Anglia in comparison to temperatures of around 11 deg C in the cloudy regions in west Wales, west Scotland and Northern Ireland.

5.3 Comparison of 09z (T+3) forecasts

The comparison of forecasts of cloud cover for the fine-mesh forecast, operational mesoscale forecast A2 and experimental forecast F2 is shown in figure 8. Figures 9 and 10 show the comparison of the forecasts of 10m wind , screen temperature , dynamic and convective precipitation and visiblity for experiments A2 to D2 and F2 to H2. There is virtually no difference in the forecasts of 10 m wind and they will not be discussed further. In order to investigate the effect near high topography of reducing the level of diffusion and any problems related to performing the diffusion of the thermodynamic variables along approximately horizontal surfaces near orography the forecasts of screen temperature, cloud cover and fog in Scotland were studied in more detail. Figures 11,12 and 13 show the comparison of forecasts A2, B2, F2 and G2 for cloud cover, screen temperature and fog respectively. To investigate the effects on the vertical structure of the forecasts cross-sections along the lines AA' and BB' shown in figures 14 were studied. Figures 15 and 17 show sections of potential temperature and vertical velocity for experiments H2, F2, D2 and A2 and figures 16 and 18 show sections of potential temperature and cloud water mixing ratio for experiments F2, B2, D2 and A2 and H2, F2, D2 and A2 respectively. The forecasts of screen temperature , rainfall , fog and vertical velocity will be compared below but first the cloud forecasts will be considered as these have impacts on the screen temperature forecasts.

5.3.1 Cloud Cover and Cloud Water Mixing Ratio

As mentioned earlier the operational mesoscale forecast produced a good forecast of the east-west contrast of screen level temperature that was better than the fine-mesh forecast verifying at the same time , see figures 6b,7 and 9a. As can be seen from figure 8 the differences in the two forecasts are largely the result of differences in cloud cover. At 09z the fine-mesh area of diagnosed full cloud cover is not as extensive as observed, the main area of diagnosed full cover being along the line of the front and not extending far enough east or westwards. The area of full cover diagnosed over East Anglia probably explains why the forecast screen temperatures in that area are lower than in reality. The mesoscale model, benefitting from its 3 hourly assimilation/forecast cycle and in particular from the 06z cloud analysis, has a reasonable forecast of total cloud cover. The region of clear skies extends slightly too far west and there are erroneous small clear areas over the Isle of Man, Irish Sea and central Scotland, The latter may be the result of a lack of observations at 06z. The effect of reducing the level of diffusion of the thermodynamic variables is to produce rougher edges to the area of full cover as seen from the comparison of figures 8b and 8d. The amount of cloud on the French coast was correctly increased and the area of cloud over the North Sea was possibly correctly extended southwards. There was also possibly an improvement in the forecast in the area of the Tees valley with more cloud in the valley than on the high ground either side.
From figures 11b and 11d it can be seen that removing the low level diffusion of the thermodynamic variables slightly reduced the amount of cloud cover from the Inverness area and Glen Mor and increased the size of the clear area in the south. However reducing the level of diffusion of those variables at all model levels has a greater impact, further reducing the amount of cloud cover in those regions, as shown in figures 11a and 11c and confirmed by the cross-sections through the Inverness area in figure 16. Comparison of figure 16 with figure 15 shows that with lower levels of diffusion of the total water the maxima in cloud water mixing ratio are more closely tied to the regions of ascent and the amounts decrease more rapidly in regions of descent.
Cross-section BB' passes through the front which lies approximately midway along the section at 09z. From figure 18 it can be seen that the maxima in cloud water are increased as the diffusion of the thermodynamic variables is reduced. A sharp maximum appears upwind of the highest peak in the orography along the section which is also just upstream of the surface front. This may be linked to the increased level of convective activity on the front although there is none actually occuring along the line of the section at 09z.
On this occasion the reduction of cloud cover with the reduction of the diffusion does not appear to improve the verification of the forecast. However the clear area in the south of Scotland was in an area containing no observations and so may be the result of an error in the initial conditions . Also the reduction of cloud cover in the Glen Mor area is to the north west of all the observations and so cannot be verified. We really need more knowledge of the accuracy of the initial cloud analysis. The depth and distribution of cloud in the initial conditions may have been incorrect.

5.3.2 Screen Temperature

The operational mesoscale forecast A2 generally predicts the strong gradients of temperature in north east England and eastern Wales well. The overall values for the country generally agree with the observations. Most of the errors are a result of incorrect forecasts of cloud cover resulting in temperatures that are too high in southern England and southern Scotland where clear skies were incorrectly predicted.
The reduction in the level of diffusion of θ_L and q_t produces greater orographic detail in the forecasts. No diffusion in the lowest three

model levels produces a tighter, better gradient in north east England and higher temperatures in Glen Mor . Removing diffusion of the thermodynamic variables at all levels also reduced temperatures over low ground in Teesdale but there are no observations to verify against. All these effects can be explained as a consequence of the changes in the cloud cover forecast discussed above.

5.3.3 Rainfall

The forecast position of the stratiform precipitation is generally good where it can be verified, although there is possibly too much drizzle ahead of the surface trough in England and Wales. Reducing the level of diffusion results in rougher precipitation fields and extends the precipitation on the front edge of the trough across the English Channel.
None of the runs predicted the showers over Ireland but reduced levels of diffusion of θ_L and q_t resulted in a lot of convection associated with the rainfall in the trough, over France and the North Sea. There was no obvious improvement in the roughness of the precipitation field when divergence damping was used rather than linear diffusion of momentum , compare D2 and H2. There was also hardly any difference between forecasts with and without diffusion of θ_L and q_t in the lowest three model levels compare A2 and B2 and F2 and G2.
Comparison with the initial conditions and fine-mesh forecast for 09z in figure 6 shows that the runs with lower values of diffusion of the thermodynamic variables have maintained more of the convective activity, in the trough, that was initialized as regions of rainfall and predicted by the fine-mesh.

5.3.4 Fog

Fog was observed on the Channel coasts, both in France and England, the south Wales mountains and off the east coast of Scotland and north east England with reduced visibility at many locations along the front. The operational mesoscale forecast A2 had fog over the North Sea, except where it had been removed by the 06z observations, and close to the north east coast of England and east coast of Scotland, in broad agreement with the observations. The mesoscale model also had areas of fog associated with the high ground in Scotland, the Pennines, Northern Ireland, The Wicklows, the moors in south west England and north and south Wales which we cannot verify with the surface observations. However there are a few observations of fog or reduced visibility that correspond with forecast fog in the above regions.
Reducing the level of diffusion in the model generally kept the areas of fog closer to the high ground, not spreading it down the slopes into the valleys. However more fog eas produced in the areas of spurious showers and extra precipitation across the English Channel and in various areas near coasts and over the sea. The production of more coastal fog on the Channel coasts was a beneficial result but it appears that the removal of low level diffusion of θ_L and q_t may be accentuating incorrect coastal effects due to the finite grid size. Comparison with figure 6 shows that runs with reduced diffusion of θ_L and q_t have retained more of the fog that was initialized at 06z, particularly in the Channel and north of the Wash.

5.3.5 Vertical Velocity

From figures 15 and 17 we see that reducing the diffusion of θ_L and q_t results in more intense vertical motion but the fields are only slightly rougher. Away from the region of the front there is little difference whether divergence damping or ordinary linear diffusion of momentum is used. However near the front, see figure 17, there are more intense narrow bands of vertical motion but that may result from more convective activity in the area.

6 Conclusion

From the active frontal case 11/4/85 it appears that there is little difference in the forecast produced with operational values of the diffusion coefficients and those produced with reduced levels of linear diffusion and divergence damping. Those with lower levels of diffusion of either type have rougher pressure, precipitation and vertical velocity fields. If the total level of diffusion of the horizontal velocity components is reduced below a certain limit the forecasts fail. The actual failure is a result of the instability caused by the production of high magnitudes of vertical velocity which violate the CFL stability criterion in the vertical

$$\text{etadot} < \Delta z / \Delta t$$

From both the 11/4/85 and 17/6/86 cases it appears that there is no obvious advantage in using divergence damping rather than linear diffusion of momentum. However the impact may be greater in longer forecasts but that has not yet been studied.

We see from the weak frontal case 17/6/86 that it is possible to remove the horizontal diffusion of the thermodynamic variables , θ_L and q_t , without the forecasts failing. Over the land more orographic detail is then seen in the low level fields , tighter gradients of the screen level temperature are produced and less cloud is produced in the valleys where there is downward motion . However the precipitation field and over the oceans and around the coast the temperature and moisture fields are then very rough . Results from forecasts on different cases run to 12 hours or more show that the level of roughness over the ocean is unacceptable by about T+9. In particular fog is produced at many locations around the coast . Forecasts run on a case study of fog in the Moray Firth on 24/4/84 with the horizontal diffusion of θ_L and q_t removed show that the production of fog around the coast is probably related to overshoots in the advection scheme which are smoothed out when diffusion is included. The roughnesses probably result from the strong land / sea contrast in surface fluxes. We note that Tapp and White 1976 smoothed the surface fluxes to remove problems with roughnesses in the forecast fields.

The study of the forecasts for the 17/6/86 case over Scotland did not conclusively show that any problems occur as a result of using the approximation to horizontal diffusion near steep orographic gradients. This was mainly because of the problems of verifying the forecasts and initial conditions. However it is clear that the forecasts are very

sensitive to the level of diffusion in these areas. Recent experience with a high vertical resolution version of the model has shown that there are definitely problems occuring due to the need to extrapolate gradients when orographic height changes are larger than the spacing of the model levels. It is obvious that some form of diffusion or smoothing is required to remove the roughnesses from the fields. It is possible to change to diffusing along eta surfaces but this is incorrect theoretically and may result in erroneous low level temperature and cloud structure as well as producing standing waves above orography. Smoothing the surface flux fields rather than fields throughout the depth of the model may help but at the expense of smoothing out the effects of local surface contrasts. A third alternative is to try using a positive definite advection scheme such as upstream differencing with corrections to reduce the level of implicit diffusion (Smolarkiewicz and Clark 1986)

Finally , it is difficult to decide on a level of diffusion for the mesoscale model. The current required levels may well be masking instabilities, boundary problems (both lateral and upper), or noise produced as a result of using grid point physics. In particular failures resulting from low levels of diffusion of momentum seem to be related to problems with the convection scheme. However as a result of the cases studied here the diffusion coefficient for the thermodynamic variables K_H has been reduced by a factor of two to 2.25×10^4 m^2 s^{-1}.

7. References

Bailey M.J. 1982 The effects of orography in a non-hydrostatic model under idealized conditions, Met O 11 Working Paper No. 37

Bell R.S. and Downton R. 1986 A trial of modified diffusion in the coarse-mesh model, Met O 11 Technical Note No. 240

Carpenter K.M. 1979 An experimant using a non-hydrostatic mesoscale model, Quart.J.R.Met.Soc., 105, 629-655.

Dumelow R.K. 1983 Some experiments in the use of divergence damping in the operational assimilation model, Met O 11 Technical Note No. 171

Dickinson A. and Gange M. 1985 Some examples of noise in fine-mesh pressure and precipitation forecasts, Met O 11 Working Paper No. 82

Machin N.A. 1983 Experiments with the UKMO mesoscale model on the 12th January 1983 Case, Met O 11 Technical Note No. 178

Parrett C.A. and Cullen M.J.P. 1984 Simulation of atmospheric hydraulic jumps in the presence of rotation and mountains, Quart.J.R.Met.Soc, 110, 147-165

Smith R.N.B. 1984a The representation of boundary layer turbulence in the mesoscale model. Part I - the scheme without changes of state, Met O 11 Technical Note No. 186

Smith R.N.B. 1984b The representation of boundary layer turbulence in the mesoscale model. Part II - the scheme with changes of state, Met O 11 Technical Note No. 187

Smolarkiewicz P.K. and Clark T.L. 1986 The multidimensional positive definite advection transport algorithm : Further development and applications, J.Comput. Phys., 67, 396-438.

Tapp M.C. and White P.W. 1976 A non-hydrostatic mesoscale model, Quart.J.R.Met.Soc., 102, 277-296.

Tripoli G.J. and Cotton W.R. 1982 The Colorado State University Three-dimensional cloud/mesoscale model-1982. Part 1: General theoretical framework and sensitivity experiments, J.Recherches Atmos., 16, 185-219.

Appendix A - Model Variables

u	westerly wind component
v	southerly wind component
w	vertical wind component
m	cloud water mixing ratio
q	humidity mixing ratio
q_t	total water mixing ratio = m + q
θ	potential temperature
θ_L	liquid water potential temperature = θ - Lm/(c_pP)
TKE	turbulent kinetic energy = 0.5(u'xu' + v'xv' + w'xw')
E	orographic height
T_s	surface temperature
T_g	ground or soil temperature
p	pressure
etadot	vertical wind component in transformed coordinates etadot = w - u(dE/dx) - v(dE/dy)
P	Exner function = $(p/1000)^{kappa}$
N	Brunt-Vaisala frequency $N^2 = \beta_T d\theta_L/deta + \beta_w dq_t/deta$
β_T	g/θ
β_w	0.608g(1+0.608q-m)
g	acceleration due to gravity
S	shear $S^2 = (du/deta)^2 + (dv/deta)^2$

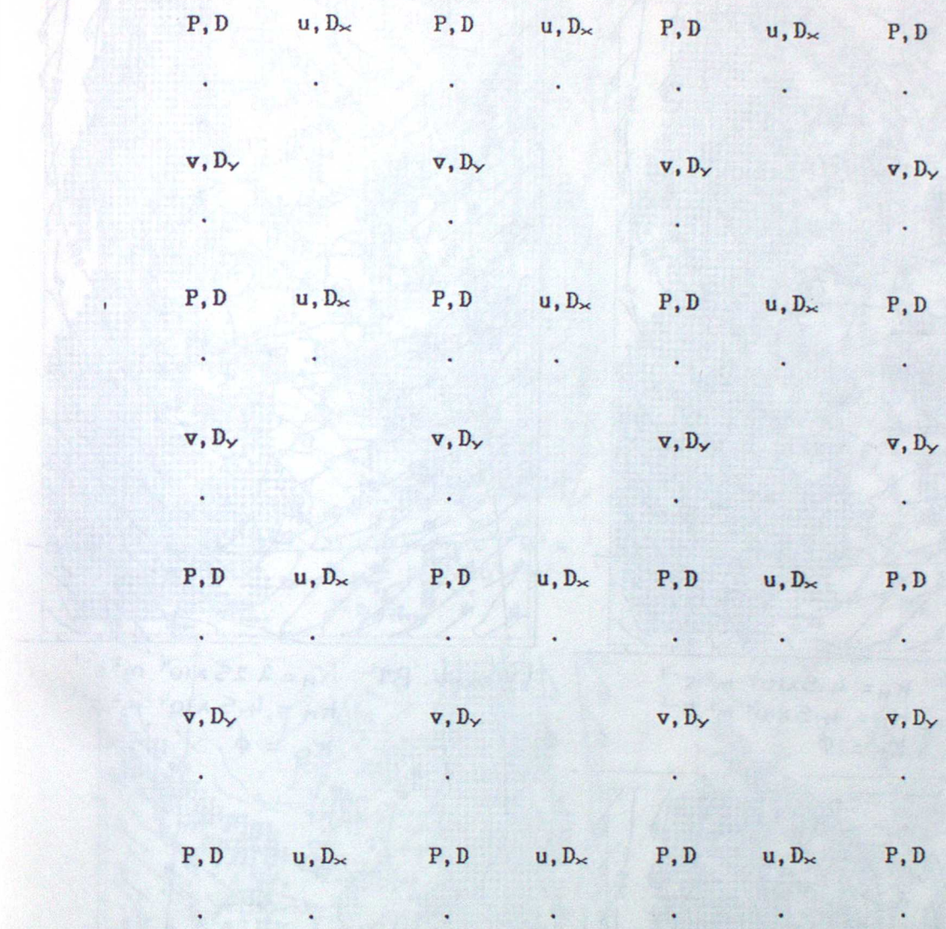

Figure 1. Positions of variables on the Arakawa C grid

P - pressure
D - divergence
D_x , D_y - gradients of divergence
u, v - horizontal wind components

Figure 2. Comparison of 3 hour forecast for 09z 11/4/85 with varying levels of horizontal diffusion and no divergence damping.

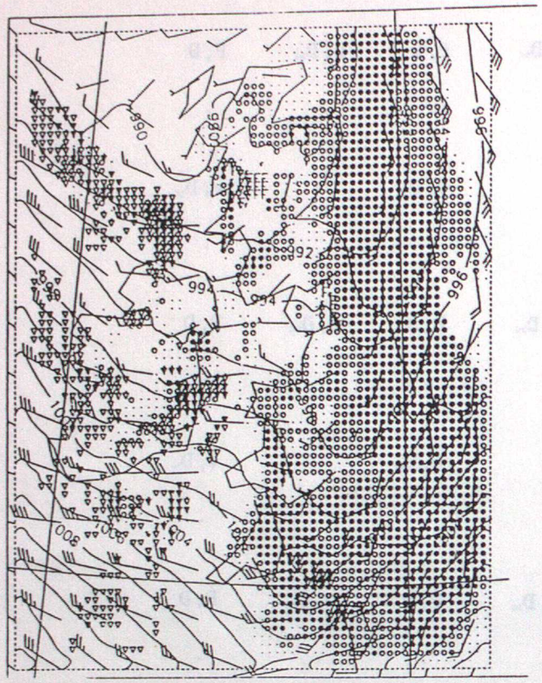

a) expt. A1 $K_H = 4.5 \times 10^4\ m^2 s^{-1}$
$K_M = 4.5 \times 10^4\ m^2 s^{-1}$
$K_D = \phi$

b) expt. B1 $K_H = 2.25 \times 10^4\ m^2 s^{-1}$
$K_M = 4.5 \times 10^4\ m^2 s^{-1}$
$K_D = \phi$

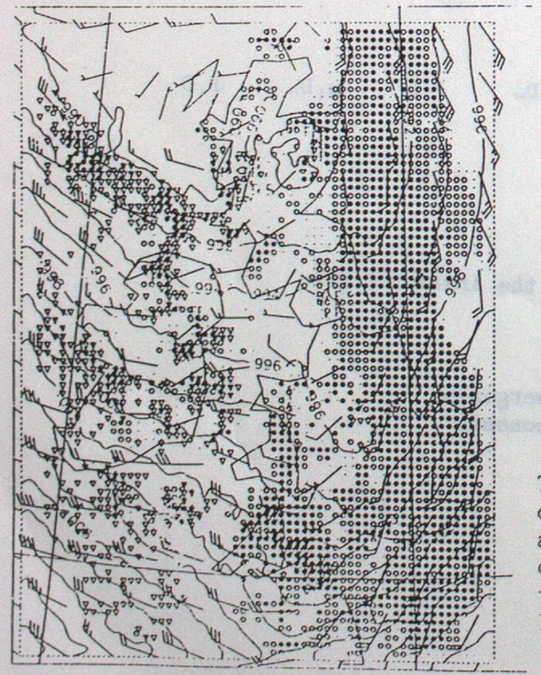

c) expt. C1 $K_H = 4.5 \times 10^3\ m^2 s^{-1}$
$K_M = 4.5 \times 10^3\ m^2 s^{-1}$
$K_D = \phi$

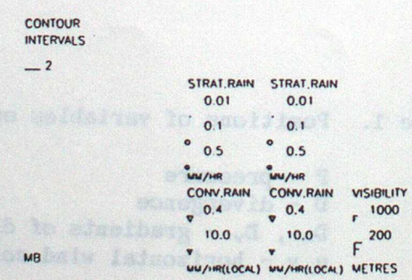

The surface charts show
contours - surface pressure at 2mb interva
arrows - wind at 10m (bottom model level)
circles - stratiform precipitation rate
triangles - convective precipitation rate
letter F - fog ie visibility less than 1km

Figure 3. Comparison of 3 hour forecast for 09z 11/4/85 with varying levels of horizontal diffusion including divergence damping.

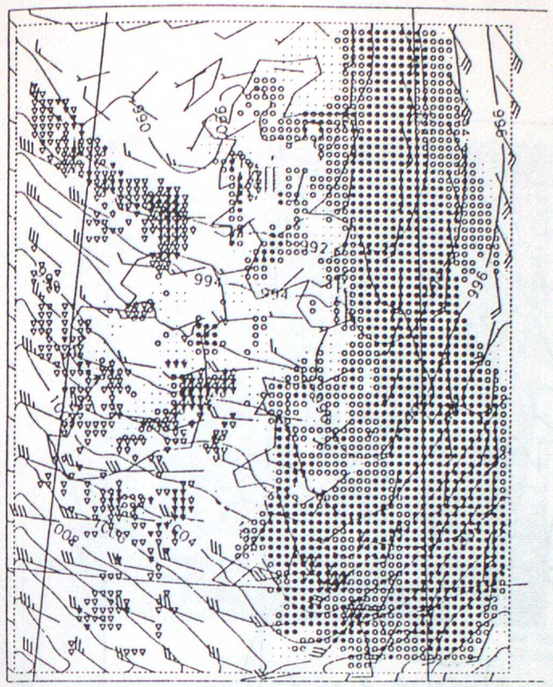

a) expt. A1 $K_H = 4.5 \times 10^4\ m^2 s^{-1}$
$K_M = 4.5 \times 10^4\ m^2 s^{-1}$
$K_D = \phi$

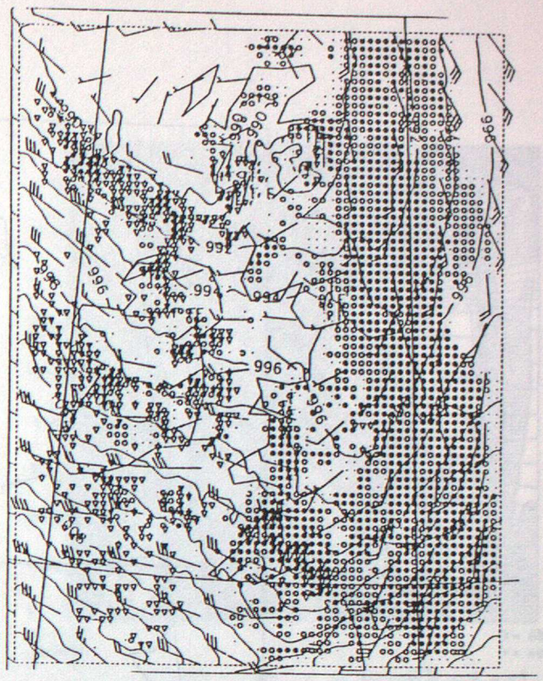

b) expt. C1 $K_H = 4.5 \times 10^3\ m^2 s^{-1}$
$K_M = 4.5 \times 10^3\ m^2 s^{-1}$
$K_D = \phi$

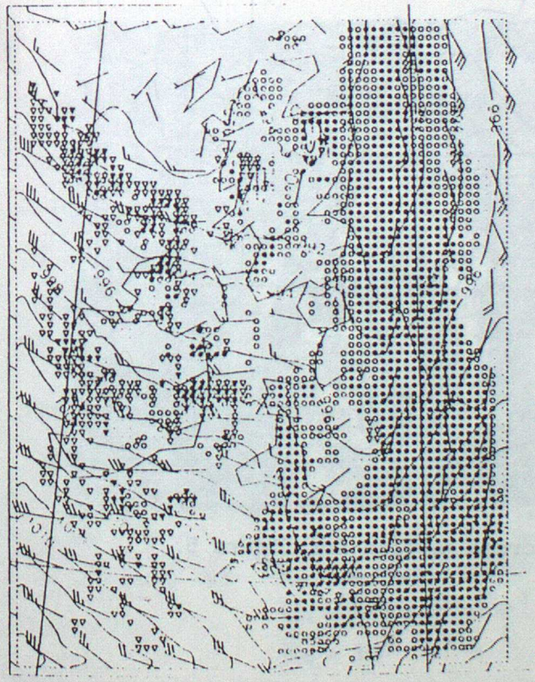

c) expt E1
$K_H = 4.5 \times 10^3\ m^2 s^{-1}$
$K_M = 4.5 \times 10^3\ m^2 s^{-1}$
$K_D = 10^5\ m^2 s^{-1}$

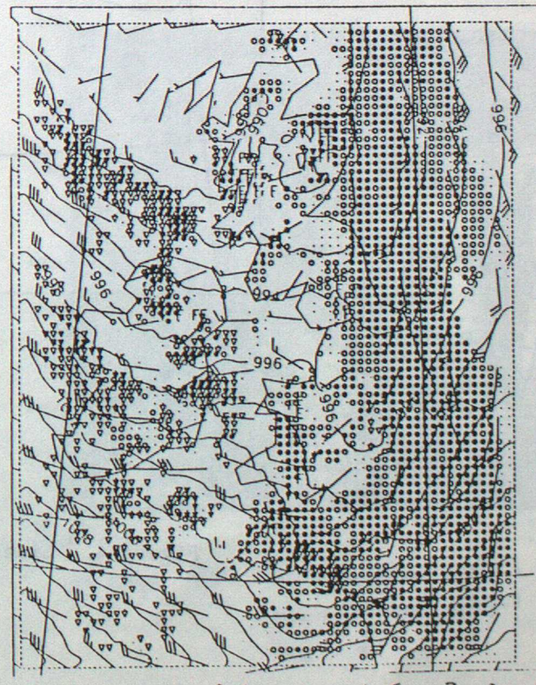

d) expt. D1 $K_H = 4.5 \times 10^3\ m^2 s^{-1}$
$K_M = 4.5 \times 10^3\ m^2 s^{-1}$
$K_D = 10^4\ m^2 s^{-1}$

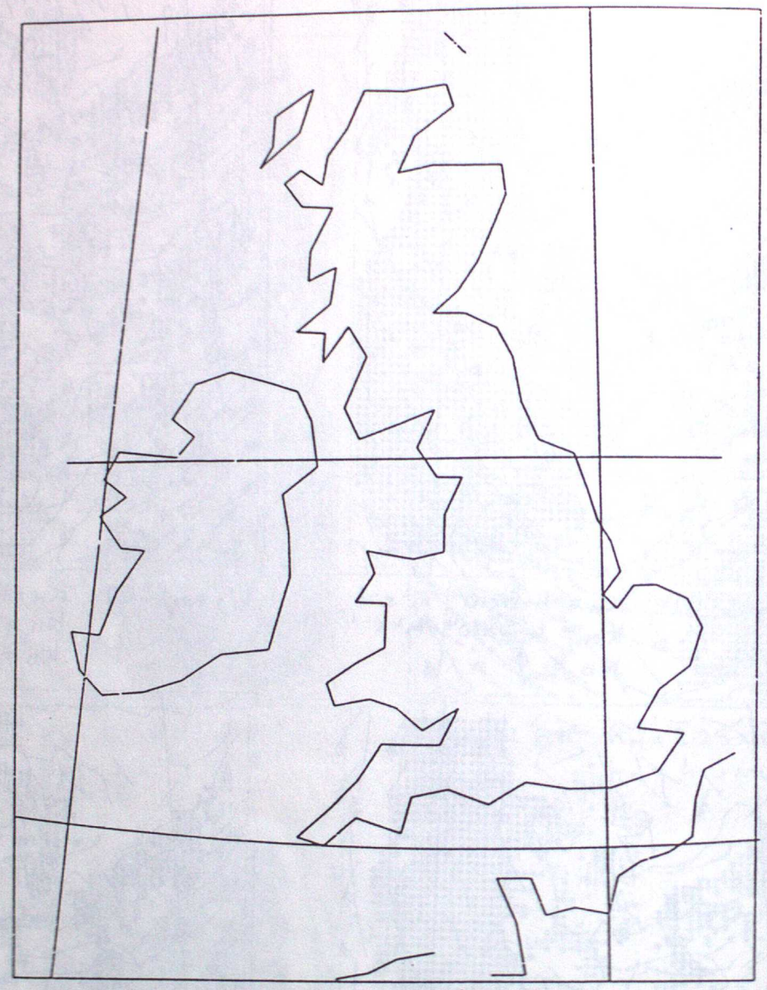

Figure 4. Line of cross-section for figure 5.

Figure 5. Comparison of cross-sections of vertical velocity, w, potential temperature, po.t , and depth of convection, c for a 3 hour forecast for 09z 11/4/85.

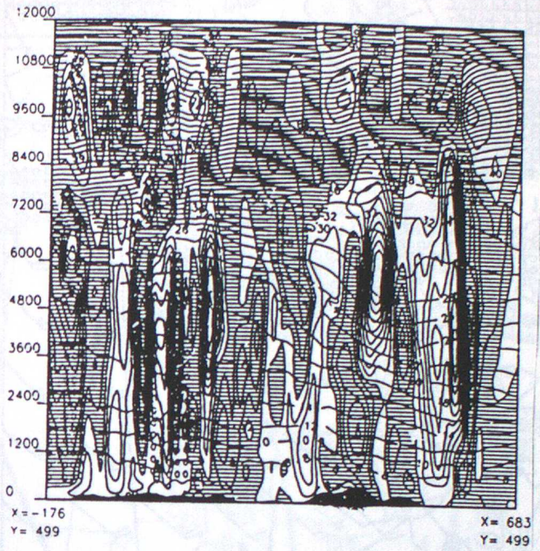

a) expt. C1 $K_H = 4.5 \times 10^3\ m^2 s^{-1}$
$K_M = 4.5 \times 10^3\ m^2 s^{-1}$
$K_D = 0$

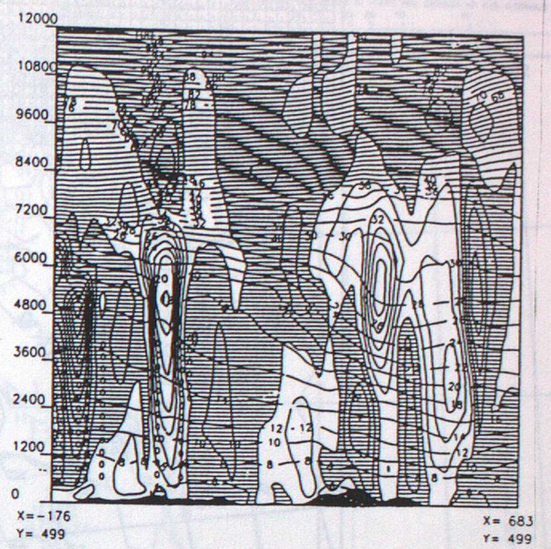

b) expt. E1 $K_H = 4.5 \times 10^3\ m^2 s^{-1}$
$K_M = 4.5 \times 10^3\ m^2 s^{-1}$
$K_D = 10^5\ m^2 s^{-1}$

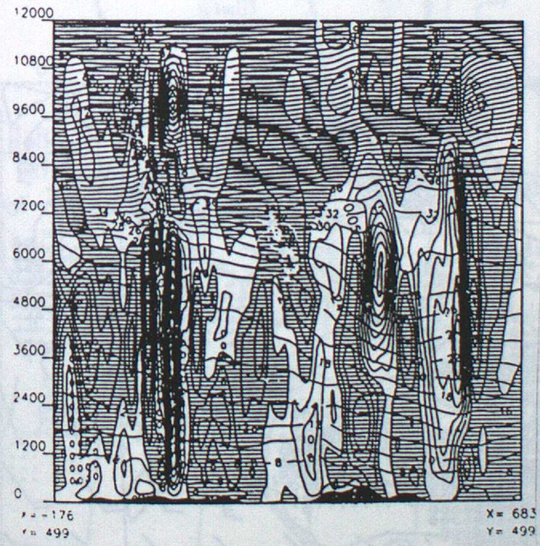

c) expt. D1 $K_H = 4.5 \times 10^3\ m^2 s^{-1}$
$K_M = 4.5 \times 10^3\ m^2 s^{-1}$
$K_D = 10^4\ m^2 s^{-1}$

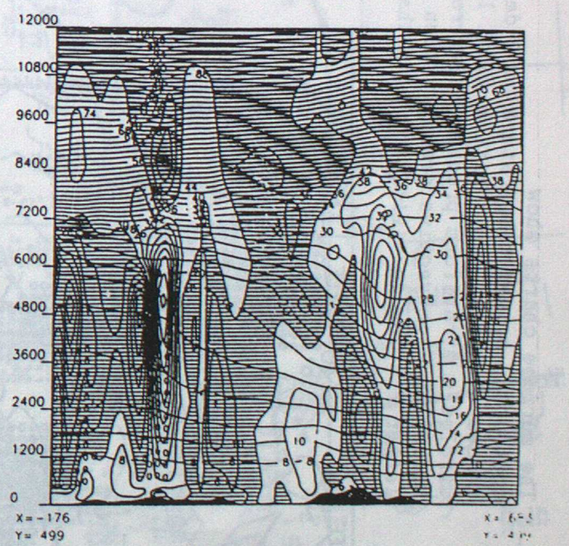

d) expt. A1 $K_H = 4.5 \times 10^4\ m^2 s^{-1}$
$K_M = 4.5 \times 10^4\ m^2 s^{-1}$
$K_D = 0$

The cross-sections show
contours - potential temperature at 2 deg C intervals
contours - vertical velocity at 0.05 ms-1 intervals with shading for downward motion
circles - convecting levels
vertical scale is height in metres
coordinates of end points of the cross-sections are metres relative to the national grid origin

Figure 6.

The surface charts show
contours - screen temperature at 2 deg C intervals
arrows - wind at 10m (bottom model level)
circles - stratiform precipitation rate
triangles - convective precipitation rate
letter F - fog ie visibility less than 1km

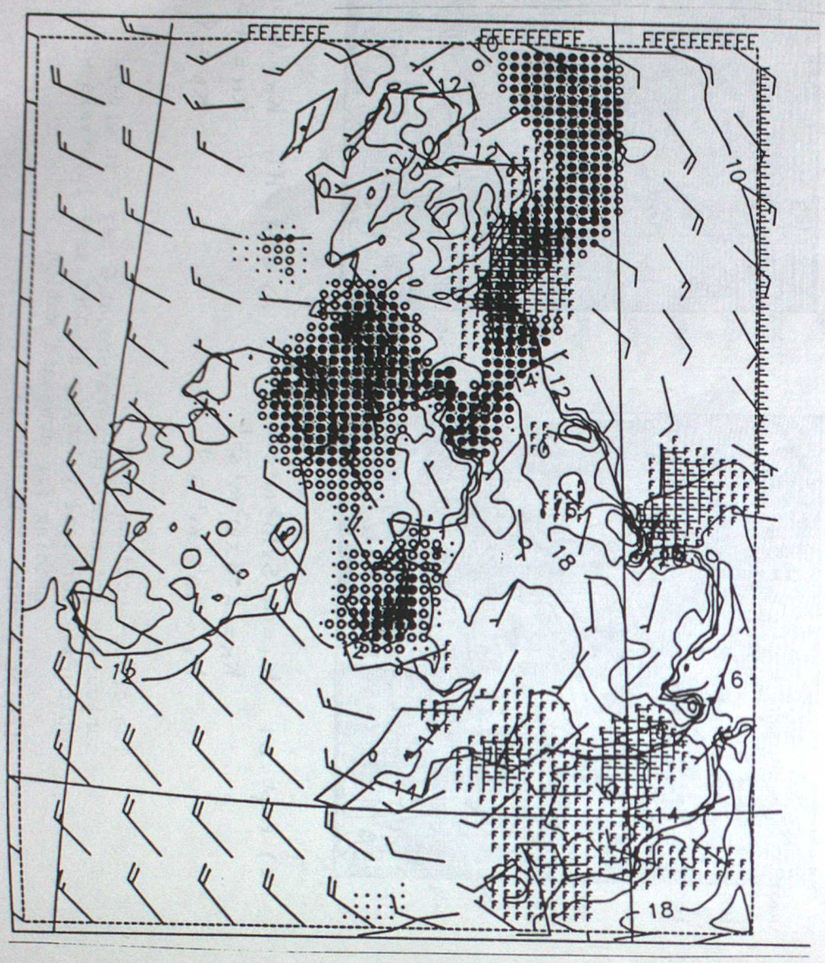

a) Initial conditions for mesoscale forecast from 06z 17/6/86

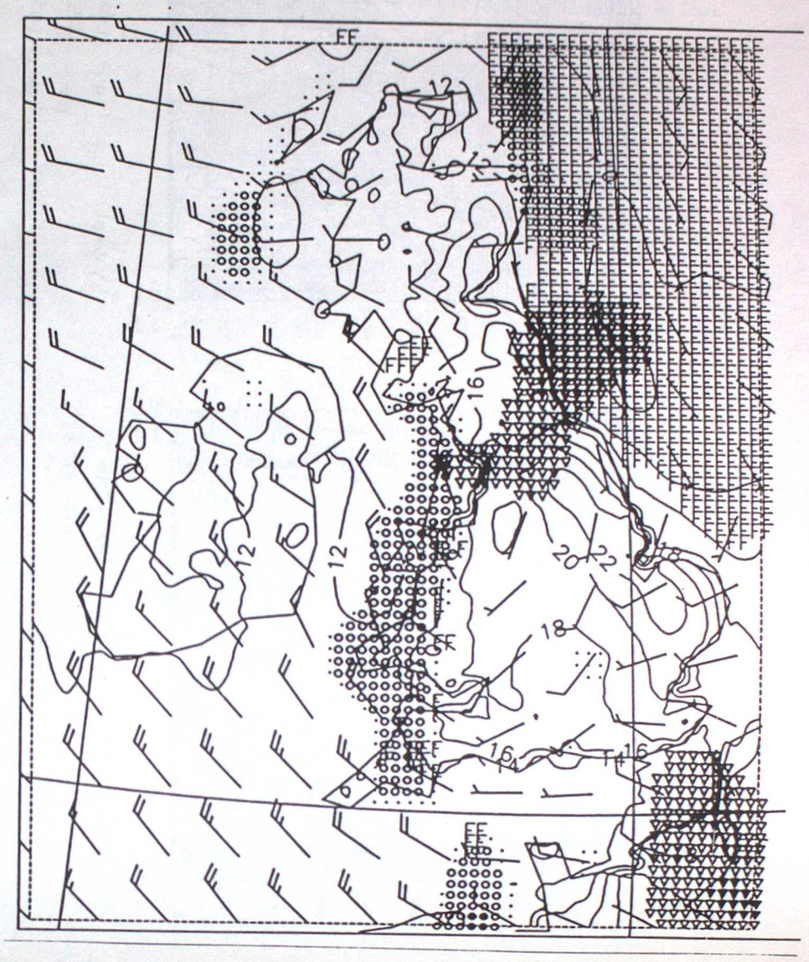

b) Fine-mesh (T+9) forecast for 09z 17/6/86

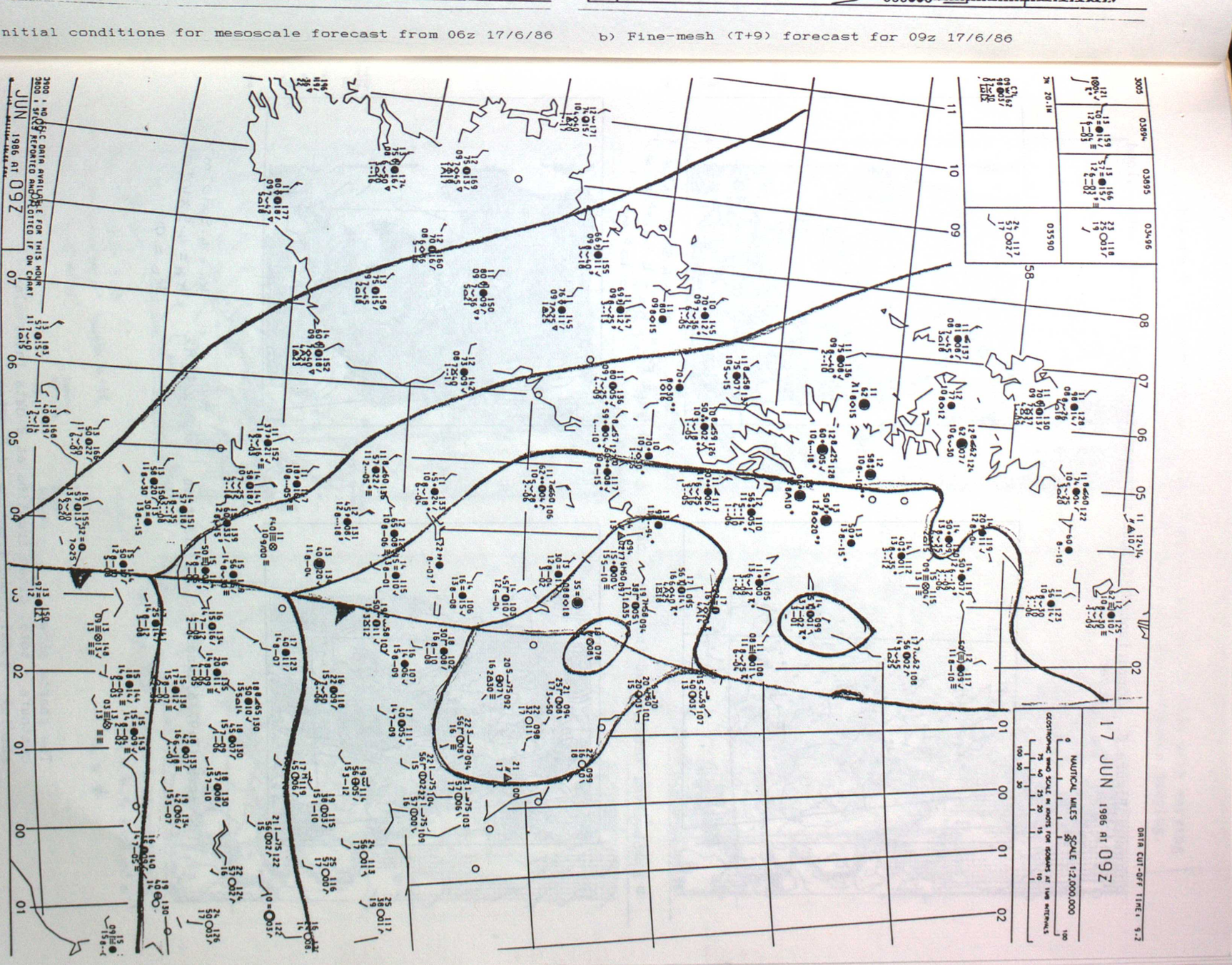

Figure 7. British Isles chart of surface observations for 09z 17/6/86 with surface pressure analysis

Figure 8. Comparison of 3 hour forecast for 09z 17/6/86 of total cloud cover.

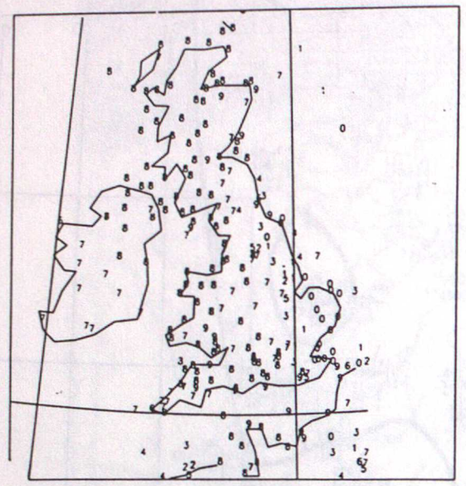

a) observed total cloud fraction - oktas

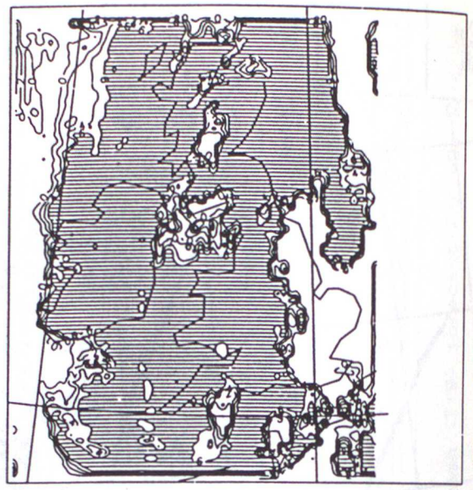

b) expt F2 $K_H = 4.5\times10^3\ m^2s^{-1}$ $K_M = 4.5\times10^3\ m^2s^{-1}$ $K_D = 10^5\ m^2s^{-1}$

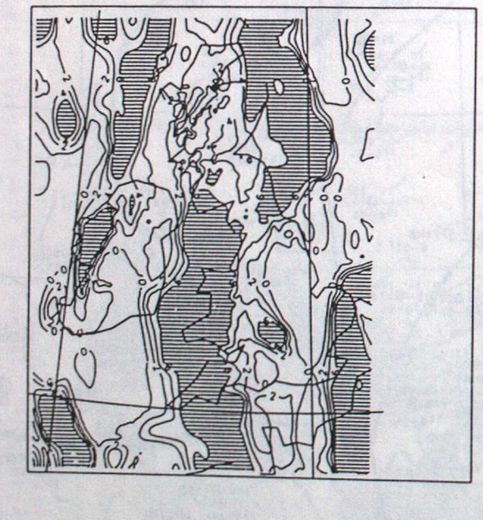

c) fine-mesh (T+9) diagnosed cloud fraction

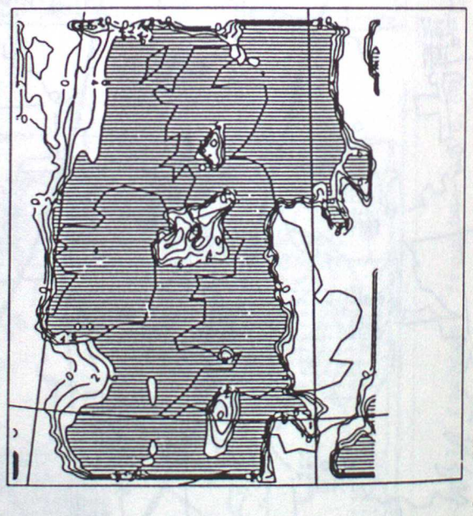

d) expt. A2 $K_H = 4.5\times10^4\ m^2s^{-1}$ $K_M = 4.5\times10^4\ m^2s^{-1}$ $K_D = \phi$

The charts show
contours - total cloud fraction at 2 okta intervals
shading - total cloud fraction of 8 oktas

Figure 9. Comparison of 3 hour forecast for 09z 17/6/86 with varying levels of horizontal diffusion and no divergence damping.

a) expt. A2 $K_H = 4.5\times10^4\ m^2s^{-1}$ $K_M = 4.5\times10^4\ m^2s^{-1}$, $K_D = \phi$

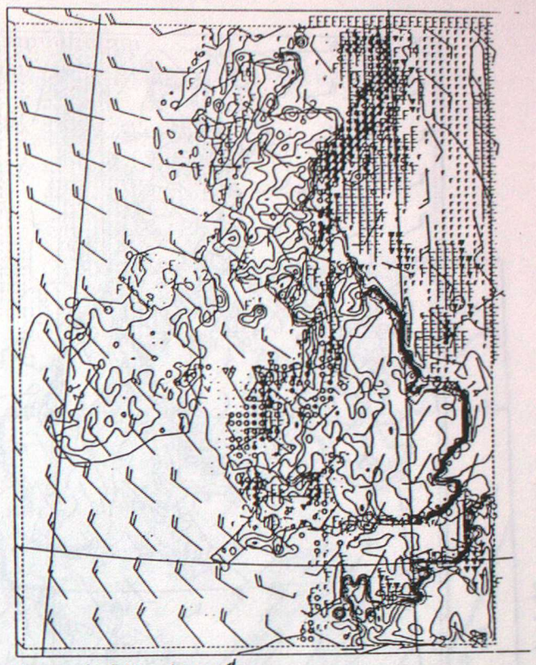

b) expt. D2 $K_H = \phi$ $K_M = 4.5\times10^4\ m^2s^{-1}$, $K_D = \phi$

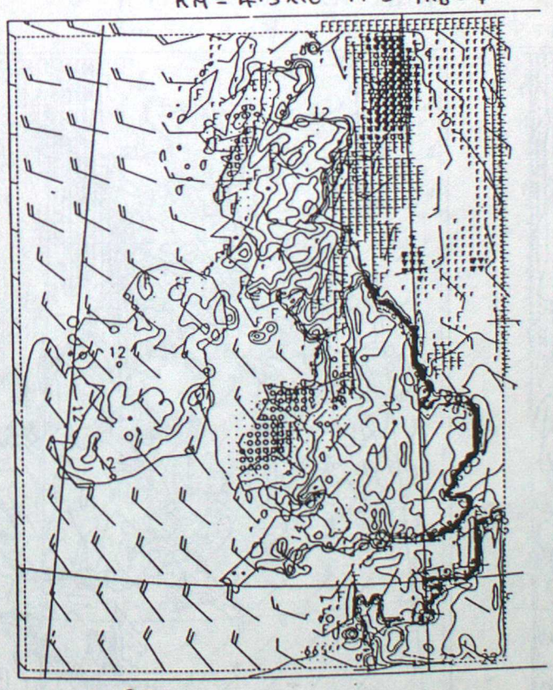

c) expt. B2
$K_H = \phi$ levels 1-3
$K_H = 4.5\times10^4 m^2s^{-1}$ levels 4-16
$K_M = 4.5\times10^4 m^2s^{-1}$
$K_D = \phi$

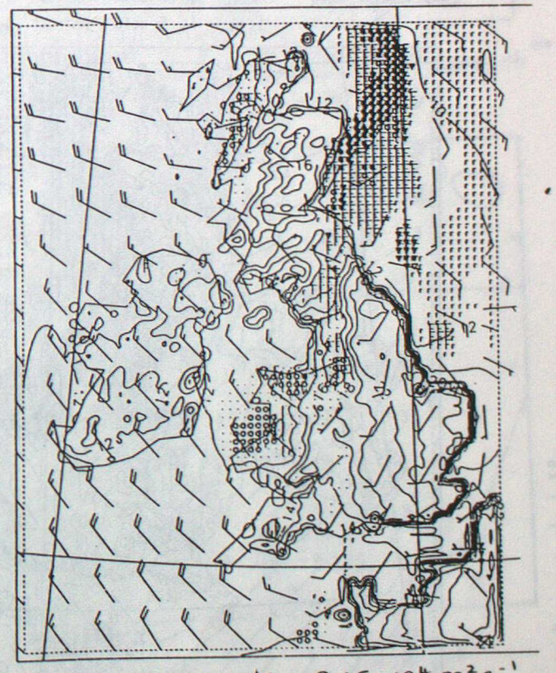

d) expt. C2 $K_H = 2.25\times10^4\ m^2s^{-1}$ $K_M = 4.5\times10^4\ m^2s^{-1}$ $K_D = \phi$

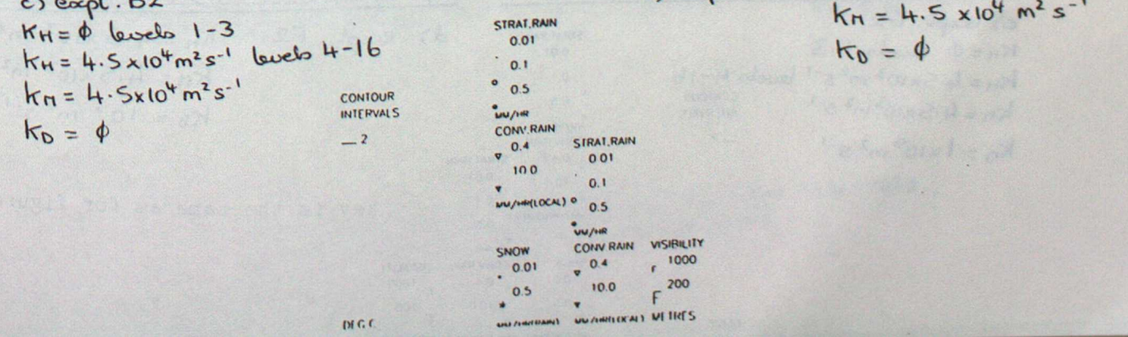

Figure 10. Comparison of 3 hour forecast for 09z 17/6/86 with varying levels of horizontal diffusion including divergence damping.

a) expt A2 $K_H = 4.5 \times 10^4\ m^2 s^{-1}$
$K_M = 4.5 \times 10^4\ m^2 s^{-1}$, $K_D = \phi$

b) expt. H2 $K_H = \phi$, $K_M = \phi$
$K_D = 10^5\ m^2 s^{-1}$

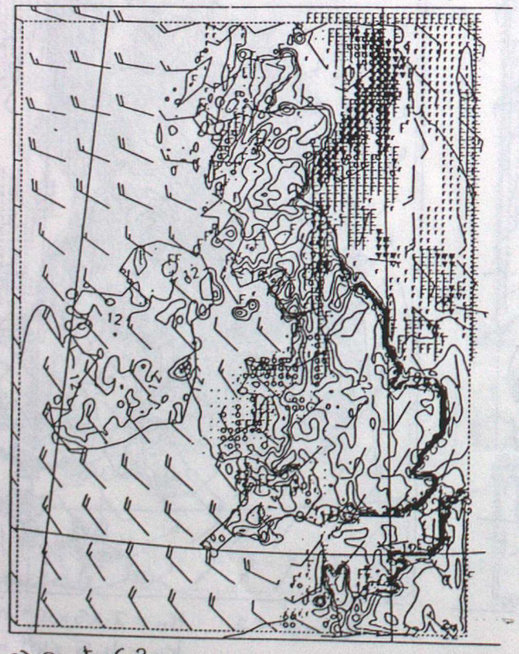

c) expt. G2
$K_H = \phi$ levels 1-3
$K_H = 4.5 \times 10^3\ m^2 s^{-1}$ levels 4-16
$K_M = 4.5 \times 10^3\ m^2 s^{-1}$
$K_D = 1 \times 10^5\ m^2 s^{-1}$

d) expt. F2 $K_H = 4.5 \times 10^3\ m^2 s^{-1}$
$K_M = 4.5 \times 10^3\ m^2 s^{-1}$
$K_D = 10^5\ m^2 s^{-1}$

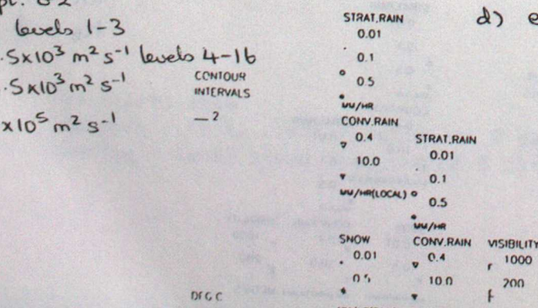

key is the same as for figure 6

Figure 11. Comparison of 3 hour forecast for 09z 17/6/86 of total cloud cover in Scotland

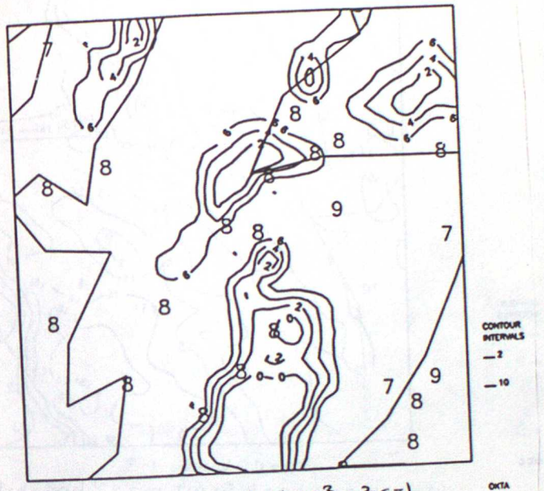

a) expt. F2 $K_H = 4.5 \times 10^3\ m^2 s^{-1}$
$K_M = 4.5 \times 10^3\ m^2 s^{-1}$
$K_D = 10^5\ m^2 s^{-1}$

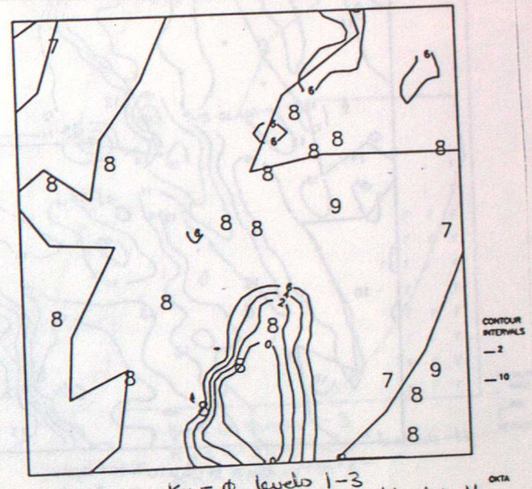

b) expt. B2 $K_H = \phi$ levels 1-3
$K_H = 4.5 \times 10^4\ m^2 s^{-1}$ levels 4-16
$K_M = 4.5 \times 10^4\ m^2 s^{-1}$
$K_D = \phi$

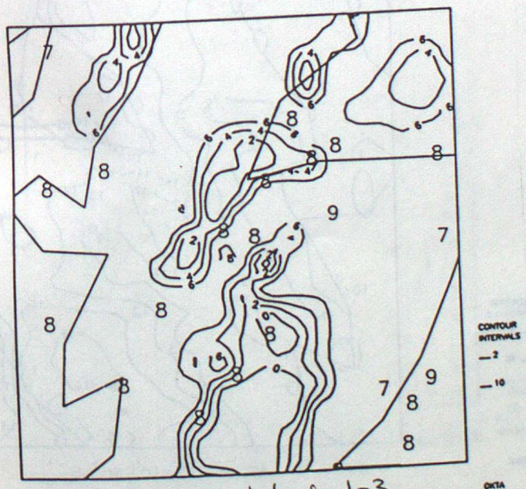

c) expt. G2 $K_H = \phi$ levels 1-3
$K_H = 4.5 \times 10^3\ m^2 s^{-1}$ levels 4-16
$K_M = 4.5 \times 10^3\ m^2 s^{-1}$
$K_D = 10^5\ m^2 s^{-1}$

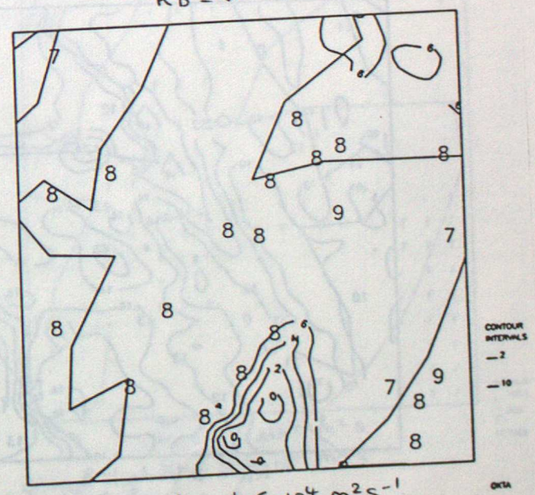

d) expt. A2 $K_H = 4.5 \times 10^4\ m^2 s^{-1}$
$K_M = 4.5 \times 10^4\ m^2 s^{-1}$
$K_D = \phi$

contours - total cloud fraction in 2 okta intervals
isolated numbers - observations in oktas

Figure 12. Comparison of 3 hour forecast for 09z 17/6/86 of screen temperature in Scotland

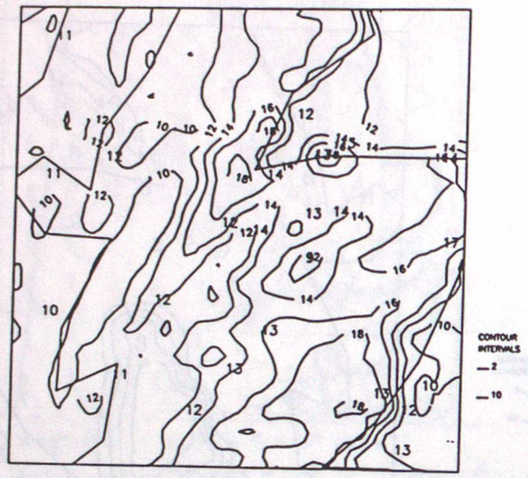

a) expt. F2 $K_H = 4.5 \times 10^3\ m^2 s^{-1}$ $K_M = 4.5 \times 10^3\ m^2 s^{-1}$ $K_D = 10^5\ m^2 s^{-1}$

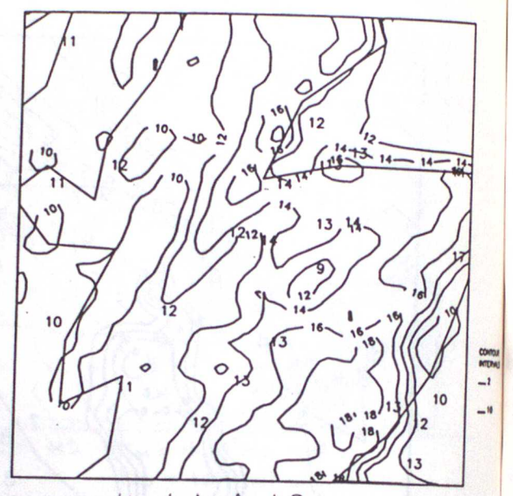

b) expt B2 $K_H = \phi$ levels 1-3 $K_H = 4.5 \times 10^4\ m^2 s^{-1}$ levels 4-16 $K_M = 4.5 \times 10^4\ m^2 s^{-1}$ $K_D = \phi$

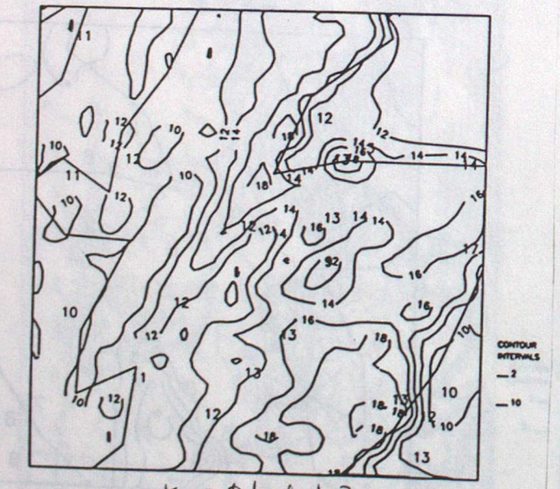

c) expt. G2 $K_H = \phi$ levels 1-3 $K_H = 4.5 \times 10^3\ m^2 s^{-1}$ levels 4-16 $K_M = 4.5 \times 10^3\ m^2 s^{-1}$ $K_D = 10^5\ m^2 s^{-1}$

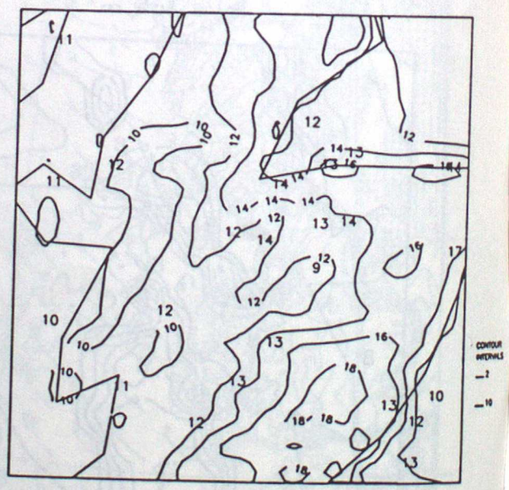

d) expt A2 $K_H = 4.5 \times 10^4\ m^2 s^{-1}$ $K_M = 4.5 \times 10^4\ m^2 s^{-1}$ $K_D = \phi$

contours - screen temperature in 2 deg C intervals
isolated numbers - observations truncated to integer deg C

Figure 13. Comparison of 3 hour forecast for 09z 17/6/86 of visibility in Scotland

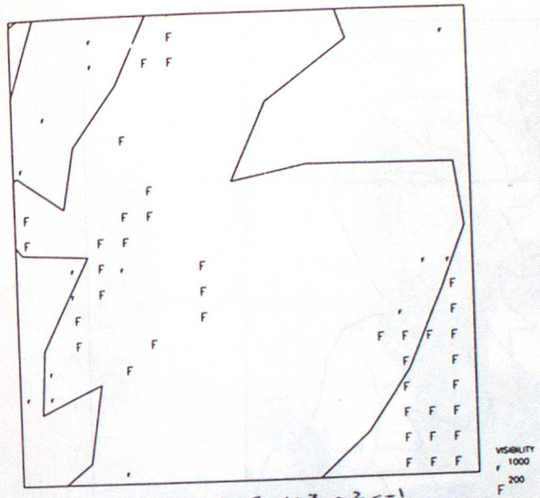

a) expt. F2 $K_H = 4.5 \times 10^3\ m^2 s^{-1}$ $K_M = 4.5 \times 10^3\ m^2 s^{-1}$ $K_D = 10^5\ m^2 s^{-1}$

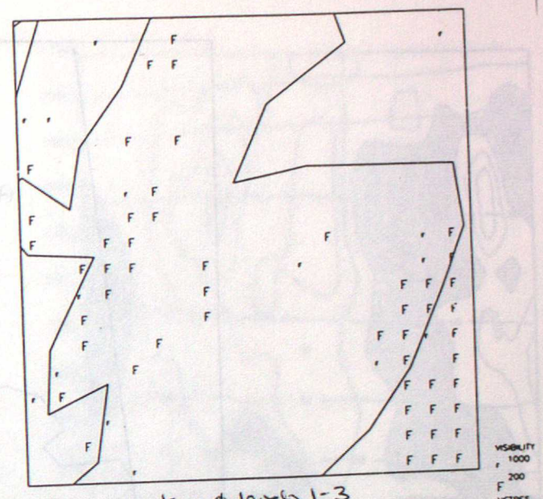

b) expt. B2 $K_H = \phi$ levels 1-3 $K_H = 4.5 \times 10^4\ m^2 s^{-1}$ levels 4-16 $K_M = 4.5 \times 10^4\ m^2 s^{-1}$ $K_D = \phi$

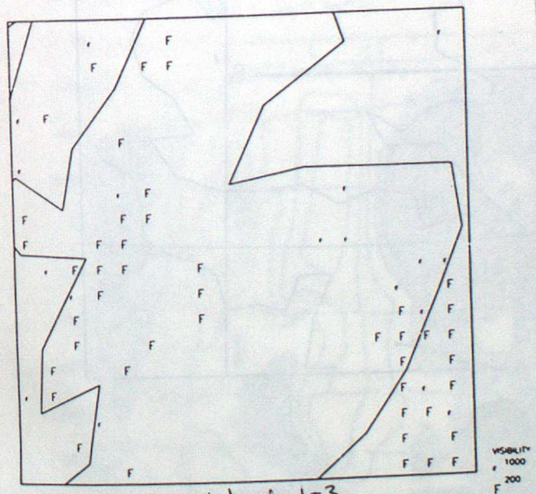

c) expt G2 $K_H = \phi$ levels 1-3 $K_H = 4.5 \times 10^3\ m^2 s^{-1}$ levels 4-16 $K_M = 4.5 \times 10^3\ m^2 s^{-1}$ $K_D = 10^5\ m^2 s^{-1}$

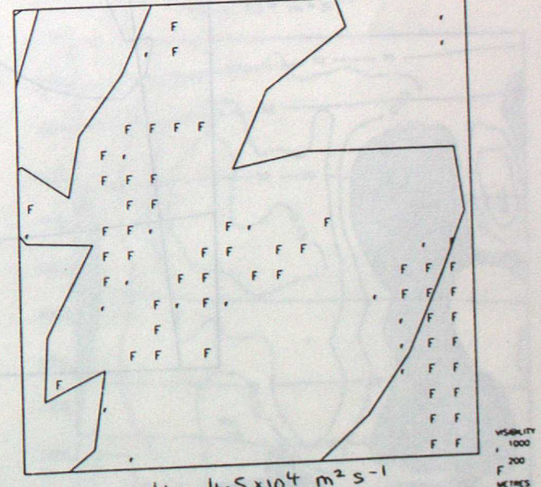

d) expt A2 $K_H = 4.5 \times 10^4\ m^2 s^{-1}$ $K_M = 4.5 \times 10^4\ m^2 s^{-1}$ $K_D = \phi$

large F - visibility < 200m , small F > 200m but < 1000m

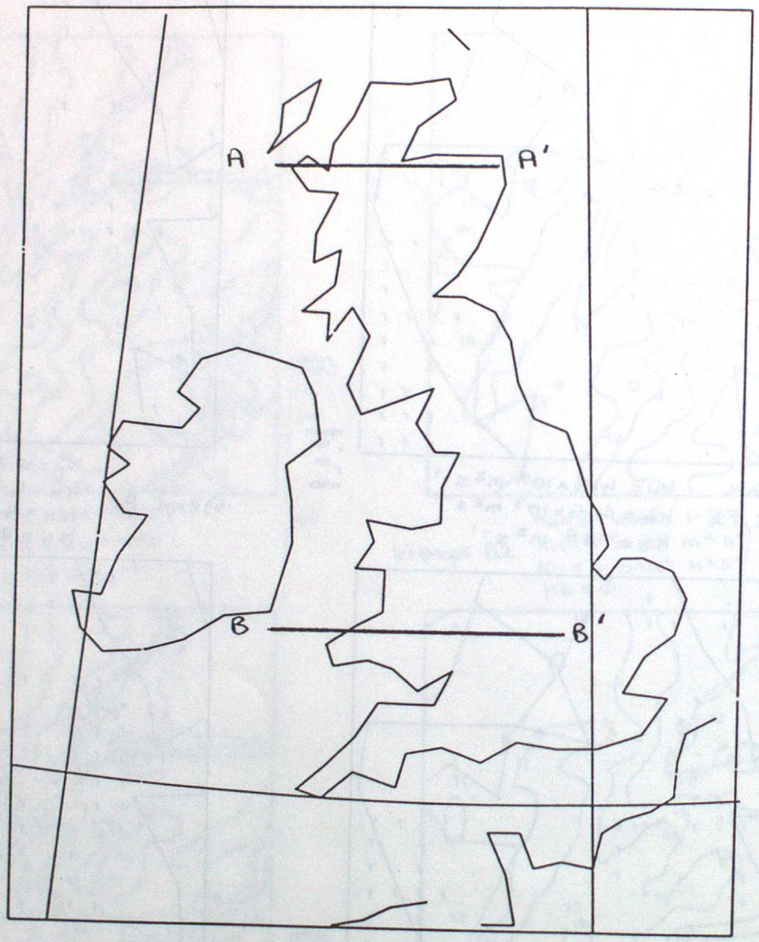

Figure 14. Lines of cross-section for figures 15 to 18.
AA' for figures 15 and 16
BB' for figures 17 and 18

Figure 15. Comparison of cross-sections of vertical velocity, w, and potential temperature, po.t , for a 3 hour forecast for 09z 17/6/86.

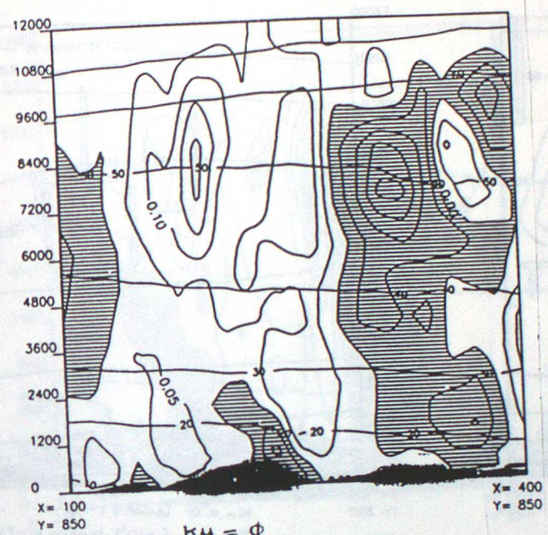

a) expt H2 $K_H = 0$, $K_M = 0$, $K_D = 10^5\ m^2 s^{-1}$

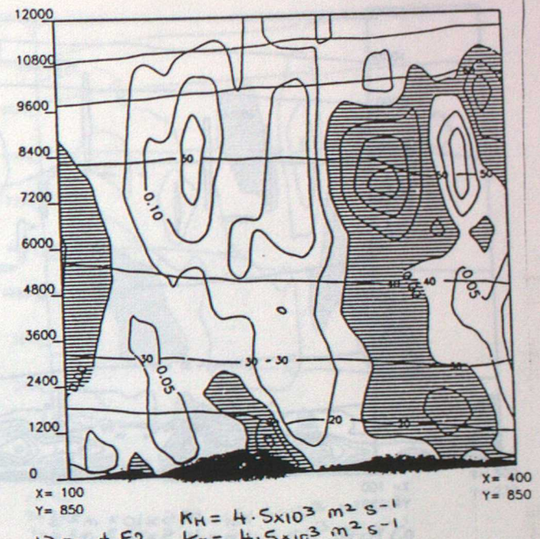

b) expt F2 $K_H = 4.5 \times 10^3\ m^2 s^{-1}$, $K_M = 4.5 \times 10^3\ m^2 s^{-1}$, $K_D = 10^5\ m^2 s^{-1}$

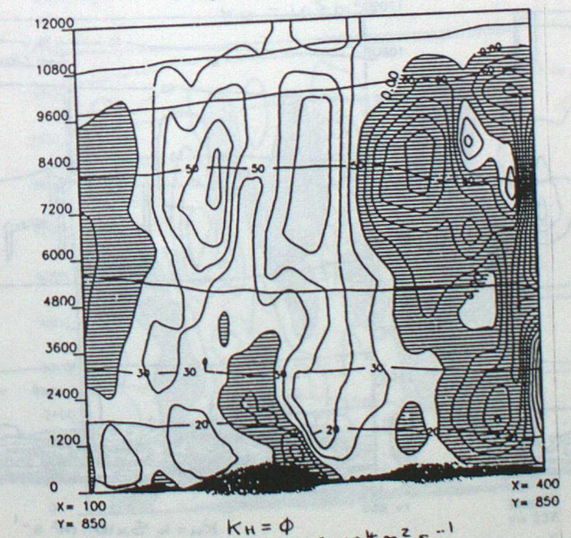

c) expt D2 $K_H = 0$, $K_M = 4.5 \times 10^4\ m^2 s^{-1}$, $K_D = 0$

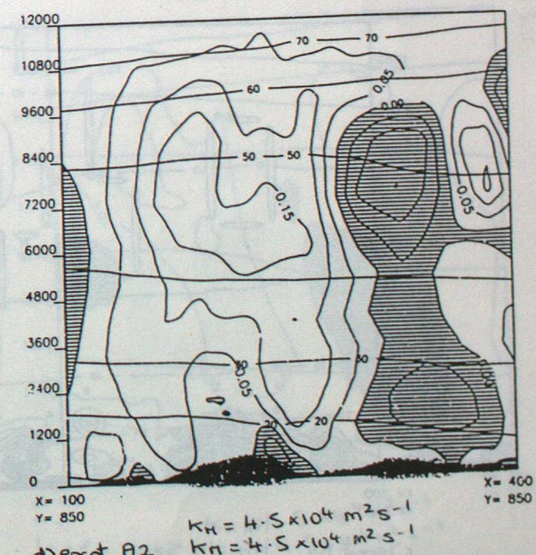

d) expt A2 $K_H = 4.5 \times 10^4\ m^2 s^{-1}$, $K_M = 4.5 \times 10^4\ m^2 s^{-1}$, $K_D = 0$

The cross-sections show
contours - potential temperature at 10 deg C intervals
contours - vertical velocity at 0.05 ms-1 intervals with shading for downward motion
horizontal and vertical scales as in figure 5

Figure 16. Comparison of cross-sections of cloud water mixing ratio , m, and potential temperature, po.t , for a 3 hour forecast for 09z 17/6/86.

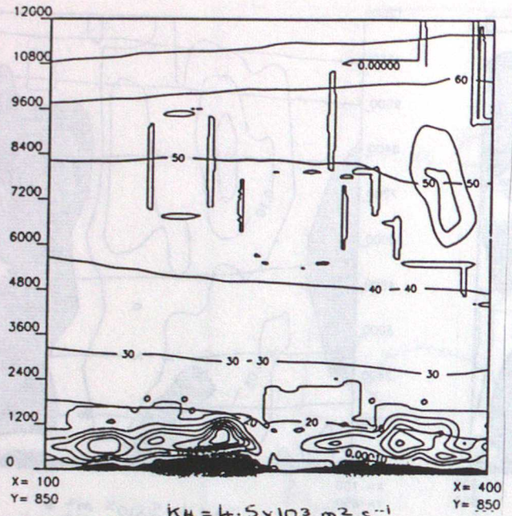

a) expt F2 $K_H = 4.5 \times 10^3\ m^2\ s^{-1}$
$K_M = 4.5 \times 10^3\ m^2\ s^{-1}$
$K_D = 10^5\ m^2\ s^{-1}$

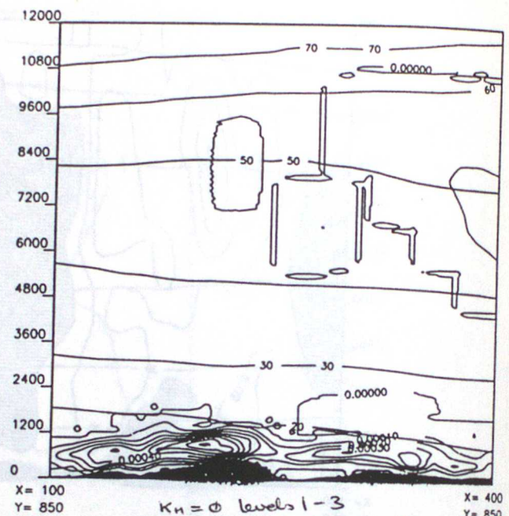

b) expt B2 $K_H = 0$ levels 1-3
$K_H = 4.5 \times 10^4$ levels 4-16
$K_M = 4.5 \times 10^4$
$K_D = 0$

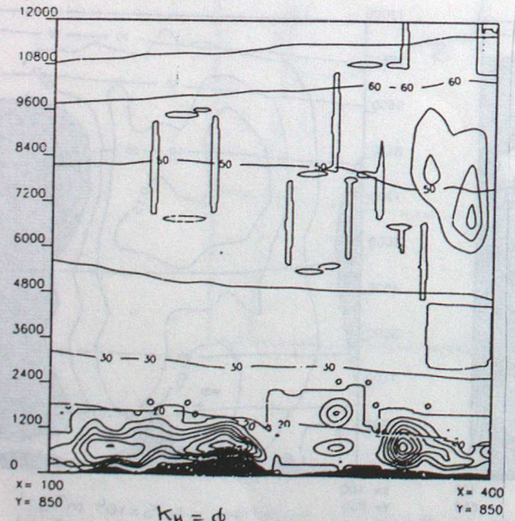

c) expt D2 $K_H = 0$
$K_M = 4.5 \times 10^4\ m^2\ s^{-1}$
$K_D = 0$

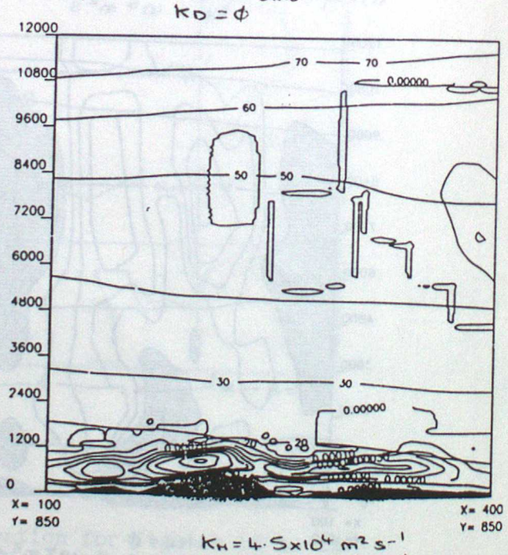

d) expt A2 $K_H = 4.5 \times 10^4\ m^2\ s^{-1}$
$K_M = 4.5 \times 10^4\ m^2\ s^{-1}$
$K_D = 0$

key as figure 15 except
contours - cloud water mixing ratio at 0.0001 kg/kg intervals

Figure 17. Comparison of cross-sections of vertical velocity, w, and potential temperature, po.t , for a 3 hour forecast for 09z 17/6/86.

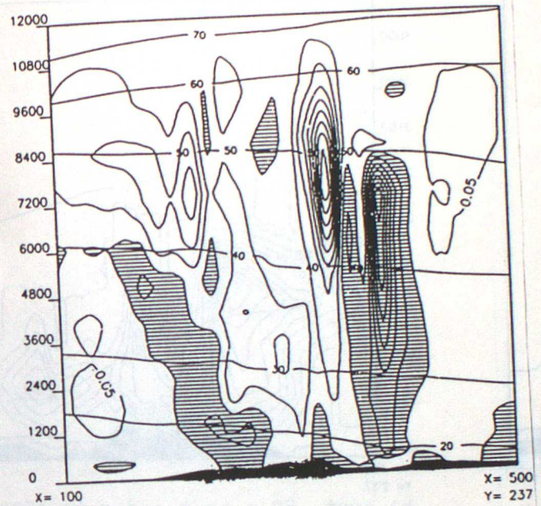

a) expt H2 $K_H = 0$
$K_M = 0$
$K_D = 10^5\ m^2 s^{-1}$

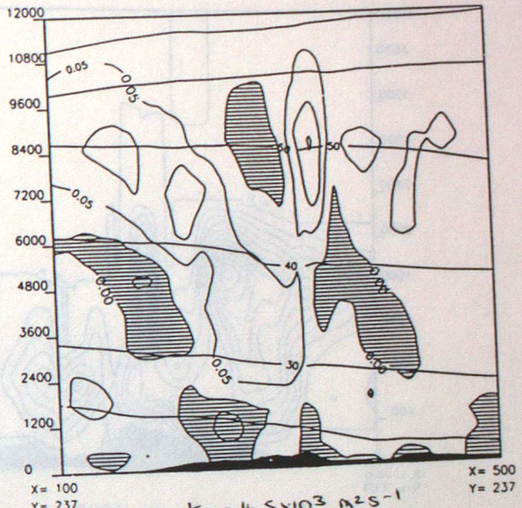

b) expt F2 $K_H = 4.5 \times 10^3\ m^2 s^{-1}$
$K_M = 4.5 \times 10^3\ m^2 s^{-1}$
$K_D = 10^5\ m^2 s^{-1}$

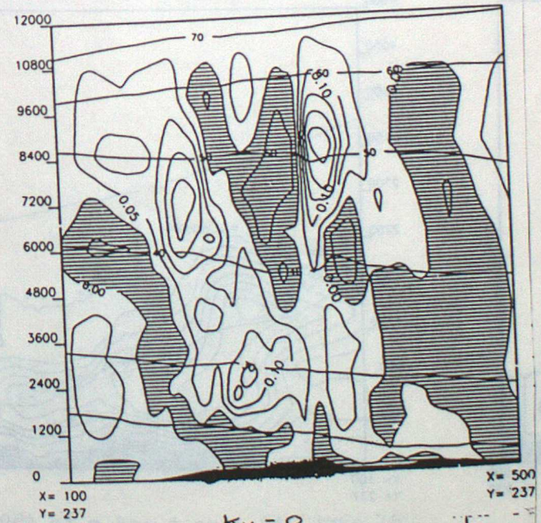

c) expt D2 $K_H = 0$
$K_M = 4.5 \times 10^4\ m^2 s^{-1}$
$K_D = 0$

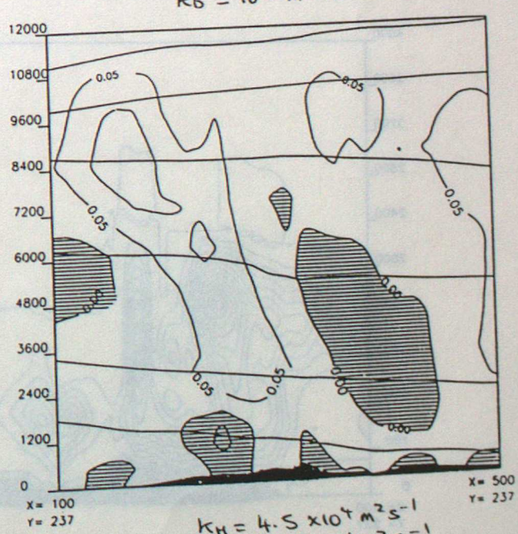

d) expt A2 $K_H = 4.5 \times 10^4\ m^2 s^{-1}$
$K_M = 4.5 \times 10^4\ m^2 s^{-1}$
$K_D = 0$

key as figure 15

Figure 18. Comparison of cross-sections of cloud water mixing ratio , m, and potential temperature, po.t , for a 3 hour forecast for 09z 17/6/86.

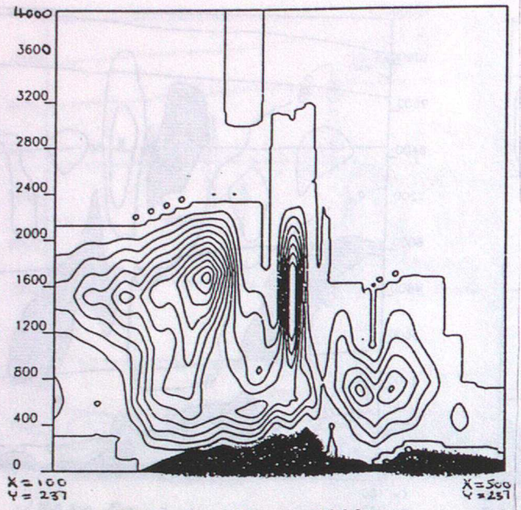

a) expt. H2 - m only to 4000m

$K_H = 0$, $K_H = 0$, $K_D = 10^5 m^2 s^{-1}$

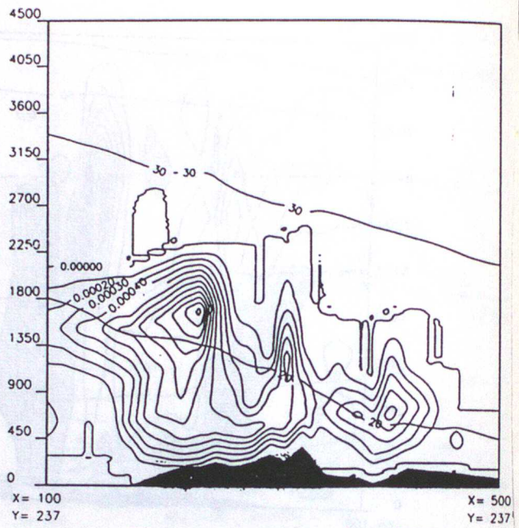

b) expt. F2 - po.t and m to 4500m

$K_H = 4.5 \times 10^3 m^2 s^{-1}$, $K_H = 4.5 \times 10^3 m^2 s^{-1}$
$K_D = 10^5 m^2 s^{-1}$

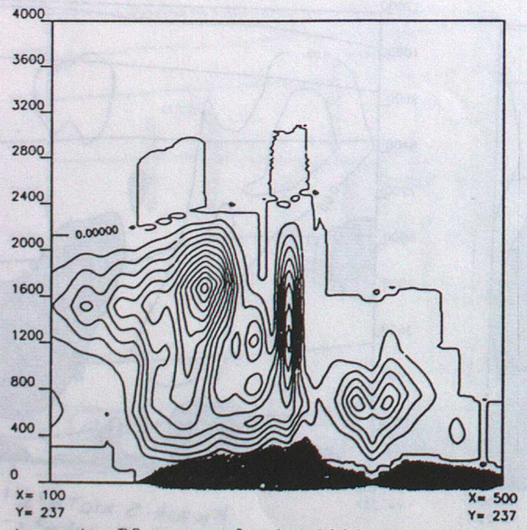

c) expt. D2 - m only to 4000m

$K_H = 0$, $K_H = 4.5 \times 10^4 m^2 s^{-1}$, $K_D = 0$

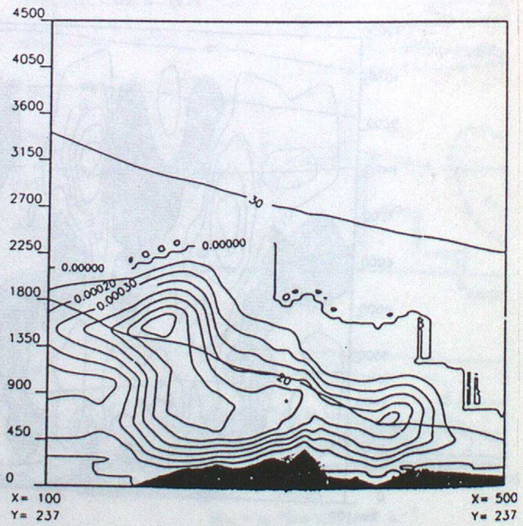

d) expt. A2 - po.t and m.to 4500m

$K_H = 4.5 \times 10^4 m^2 s^{-1}$, $K_H = 4.5 \times 10^4 m^2 s^{-1}$
$K_D = 0$

key as figure 16